Journal of Solid State Chemistry 183 (2010) 2609–2615

Contents lists available at ScienceDirect

Journal of Solid State Chemistry

journal homepage: www.elsevier.com/locate/jssc

Controllable fabrication of platinum nanospheres with a polyoxometalate-assisted process

Guoying Sun [b], Qiuyu Li [a], Rui Xu [a], Jianmin Gu [a], Mingliang Ju [a], Enbo Wang [a,*]

[a] Key Laboratory of Polyoxometalate Science of Ministry of Education, Department of Chemistry, Northeast Normal University, Ren Min Street No. 5268, Changchun, Jilin 130024, PR China

[b] Chemistry and Life Science School, Changchun University of Technology, Yan An Street No. 17 , Changchun, Jilin 130024, PR China

ARTICLE INFO

Article history:
Received 1 February 2010
Received in revised form
26 August 2010
Accepted 30 August 2010
Available online 15 September 2010

Keywords:
Platinum
Nanosphere
Polyoxometalate
Electrocatalytic

ABSTRACT

Pt nanospheres with an average diameter of 60 ± 10 nm have been successfully synthesized at room temperature through a facile polyoxometalate(POM)-assisted process. Characterization by scanning electron microscopy (SEM) and transmission electron microscopy (TEM) clearly showed that these Pt nanospheres consisted of 2–7 nm Pt nanodots. During the formation of such unique nanostructures, POMs were found to serve as both catalyst and stabilizer. The size of the as-synthesized Pt nanospheres could be controlled solely by adjusting the molar ratio of POMs to H_2PtCl_6. A possible formation mechanism based on POMs-mediated electron transfer from ascorbic acid (AA) to $PtCl_6^{2-}$ and AA-assisted aggregation was tentatively proposed to rationalize the formation of such nanostructures. Importantly, these specific Pt nanospheres exhibited good electrocatalytic activity towards the oxidation of methanol, making them promising for applications in direct methanol fuel cells.

1. Introduction

Platinum nanostructured materials have been the focus of intensive research primarily due to the increasing demand for high performance catalysts in practical applications that range from methanol oxidation and oxygen reduction in fuel-cell technology to three-way automobile catalytic conversion and hydrogenation reactions [1,2]. Driven by such demand, various chemical protocols have been developed to prepare platinum nanostructures with controlled shapes, including nanoparticles, nanowires, nanodentrites, hollow spheres, and mesoporous structures [3–7]. However, most of these methods require the use of surfactants as templates or the polyol process [8]. Recently, it has been reported that polyoxometalates (POMs), a unique class of molecular metal–oxygen clusters, can act as reducing agent for the preparation of nanostructures [9–14]. Compared with widely used organic surfactants and polymers, POMs are completely hydrophilic and very soluble in polar solvents because of their negative charges and water ligands that are chemically bonded to the external surface of POMs [15]. The absorbed anionic POMs can provide negative charges to the nanoparticles, thus preventing the aggregation of nanoparticles via strong electrostatic repulsion. In particular, POMs can not only gain, but also donate electrons while keeping their structure unchanged [16]. Such reversible charge transfer characteristics make them very attractive for the fabrication of novel nanostructured materials by homogeneous-phase electron exchange reactions. Therefore, POMs have been successfully introduced into the morphology-controlled synthesis of nano/microstructures. For example, Lee et al. have demonstrated that silicon nanostructures from quantum dots to nanowires can be successfully synthesized by POM-assisted electrochemical etching method [16]. Our group has established that carbon nanotube and nanobelt [17], hematite hollow microspheres [18], iron oxide nanorods [19] and ZnO hollow nanospheres [20,21] can be reproducibly synthesized by a simple POMs-assisted hydrothermal or solvothermal route. POMs, as reducing and capping agents, have been popularly employed to fabricate metal nanostructures [13,22–27]. However, it is well known that POMs are one class of excellent catalysts owing to their unique electronic characteristics and structural robustness, especially as strong acid catalyst, which has been used in esterification reactions [28]. Therefore, we expect that POM as an electron-transfer mediator could give extra control over the reaction process for forming metal nanostructures, which will be of particular importance for designing novel metal nanostructures.

To achieve the above aim, a typical Keggin-type POM $H_4SiW_{12}O_{40}$ (HSiW) was used as assisting agent for reducing H_2PtCl_6 via ascorbic acid (AA) under mild conditions. The overall process involved an one-electron reduction of HSiW with AA (Eq. (1)) and a re-oxidation of the reduced POMs with the metal

* Corresponding author. Fax: +86 431 85098787.
E-mail addresses: wangeb889@nenu.edu.cn, wangenbo@public.cc.jl.cn (E. Wang).

0022-4596/$ - see front matter © 2010 Elsevier Inc. All rights reserved.
doi:10.1016/j.jssc.2010.08.039

cations to yield the metal nanospheres (Eq. (2)).We demonstrated that POMs acted as both catalyst and stabilizer during the formation of Pt nanospheres, which may be important in understanding the physical process involved. Such a POM-assisted approach provided facile entry to producing of large-scale Pt nanospheres. Different from previous studies, this method required neither the application of drastic conditions, such as UV light, microwave or high temperature, nor the presence of any toxic organic contaminants in the synthesis system. On the other hand, the oxidized POMs were directly employed as assisting agent in this case, thus avoiding the complicate process to synthesize the reduced POMs

$$2SiW_{12}^{VI}O_{40}^{4-} + C_6H_8O_6 \rightarrow 2SiW_{11}^{VI}W^{V}O_{40}^{5-} + C_6H_6O_6 + 2H^+ \quad (1)$$

$$4SiW_{11}^{VI}W^{V}O_{40}^{5-} + PtCl_6^{2-} \rightarrow Pt^0 + 4SiW_{12}^{VI}O_{40}^{4-} + 6Cl^- \quad (2)$$

$$PtCl_6^{2-} + 2C_6H_8O_6 \rightarrow Pt^0 + 2C_6H_6O_6 + 4H^+ + 6Cl^- \quad (3)$$

2. Experimental section

2.1. Materials

All chemicals (analytical grade) were purchased from Aldrich and used without further purification. Nafion (perfluorinated ion-exchange resin, 5 wt% solution in a mixture of lower aliphatic alcohols and water) was purchased from Aldrich. Water used throughout all experiments was purified with Millipore system.

2.2. Synthesis of large platinum nanospheres

A typical preparation of platinum colloid was prepared as follows: 10 mL of 9.65×10^{-4} M H_2PtCl_6 aqueous solution was mixed with 4.5 mL of 10 mM HSiW aqueous solution. Next, 1.5 mL of 100 mM freshly prepared AA was added. Within 5 min, the light yellow color of the platinum solution changed to the blue color of heteropoly blue. After stirring for 3 h at 25 °C, the color of the solution turned to black, suggesting the formation of platinum nanoparticles. The control experiment was performed without the addition of HSiW. The resultant product was separated by centrifugation. Finally, the products were dispersed in water to obtain suspensions for further characterization.

2.3. Characterization

SEM measurements were made on a XL30 ESEM FEG scanning electron microscope. TEM measurements were made on a Hitachi-7500 transmission electron microscope operated at an accelerating voltage of 120 kV. X-ray diffraction patterns (XRD) were measured using a Rigaku D/max-IIB X-ray diffractometer at a scanning rate of 4°/min with 2θ ranging from 10° to 90°, using Cu$K\alpha$ radiation ($\lambda = 1.5418$ Å). X-ray photoelectron spectroscopy (XPS) measurement was performed on an ESCALAB-MKII spectrometer (VG Co., United Kingdom) with Al$K\alpha$ X-ray radiation as the X-ray source for excitation. The Pt substrates for SEM and XRD characterization were prepared by placing several drops of the suspension on silica and quartz wafers, respectively, allowing the solvent to slowly evaporate at room temperature. The sample for TEM measurement was similarly prepared by placing a drop of the suspension onto a carbon-coated copper grid. The sample for XPS characterization was dropped on glass plate. Analysis for Pt and W were performed by ICP-AES using a POMES TJA inductively coupled plasma mass spectrometer.

2.4. Electrochemical measurements

All electrochemical experiments were performed in a traditional three-electrode electrochemical cell with a CHI 842 electrochemical workstation (CH Instruments, Chenhua Co., Shanghai, China) at room temperature (~25 °C). Ag/AgCl (saturated KCl) electrode and a platinum wire were used as reference and counter electrode, respectively. The Pt nanosphere-modified glassy carbon (GC) acts as working electrode. The GC (3 mm diameter) electrode was polished before each experiment with alumina powder, respectively, rinsed thoroughly with doubly distilled water, then washed successively with 1:1 nitric acid, acetone and doubly distilled water in ultrasonic bath and dried in air. For CH_3OH electrocatalytic oxidation reaction, the amount of Pt was adjusted to 0.75 mg mL^{-1} by centrifugation and redispersing in water. The 6 μL of Pt nanosphere suspension or 6 μL 1.88 mg mL^{-1} Pt/C catalyst (40 wt% Pt, JM Corporation) solution with the same Pt loadings was dropped onto the surface of GC electrode, and dried under an infrared lamp. Then, 2 μL of Nafion (0.5%) was dropped on the surface of above modified electrode. The electrolyte solution was a 0.5 M H_2SO_4 and 0.5 M H_2SO_4+1.0 M CH_3OH solution that was prepared from high-purity sulfuric acid, high-purity grade methanol, and distilled water. All CVs were performed at a scan rate of 100 mV/s. For the characterization of HSiW electrocatalytic activity, the amount of POMs was 4.4 mg mL^{-1}, and the process was same to that of Pt nanospheres.

3. Results and discussion

3.1. Characterization of platinum nanospheres

Fig. 1a showed typical SEM image of the as-prepared sample. It was noticed that a large amount of nanospheres with an average diameter of 60 ± 10 nm could be produced through the proposed strategy. The corresponding high-magnification SEM image (Fig. 1b) revealed that the surface of each spheres was not smooth but rough, implying that these nanospheres could be comprised of smaller subunits. TEM examination was performed to confirm such a structural characteristic. As observed in Fig. 1c, these nanospheres possess good near monodispersity and rough surface. A closer look at Fig. 1d revealed an interesting feature that each nanospheres were indeed 3D structured assemblies of 2–7 nm nanodots. HRTEM images from the edge of individual Pt nanosphere showed that these small nanodots were single-crystalline (Fig. 2). From the enlarged images Fig. 2b, d of Fig. 2a, c, the {111} and {200} facets could be identified. The SAED pattern (inset of Fig. 1c) showed several clear diffraction rings, which could be assigned to (111), (200), (220) and (311) planes of face-centered cubic (fcc) metal platinum, respectively. According to the ratio of Pt amount before and after three times centrifugation, the yield of Pt nanospheres was determined by ICP-AES to be 95.7 wt%. Additionally, the W and Pt weight ratio (W/Pt) was quantified by ICP-AES to be 0.4:100.

The XRD pattern of the as-prepared sample was shown in Fig. 3. Four diffraction peaks at $2\theta = 39.8$, 46.6, 67.7 and 83.0 could be indexed to the (111), (200), (220) and (311) crystalline planes of platinum with the fcc structure (JCPDS no. 04-0802), consistent with the result determined from SAED. The nanometer size of the nanodots was evidenced by the broad X-ray reflections. According to Scherrer's equation ($D = K\lambda/(B(\cos\theta))$) from the full width at half maximum (fwhm) of (111) [29], the average size of nanodots was calculated to be about 5.2 nm, similar with the value determined from SEM and TEM. The cell parameter was calculated to be 0.390 and 0.392 nm by TEM and XRD, respectively, which was well

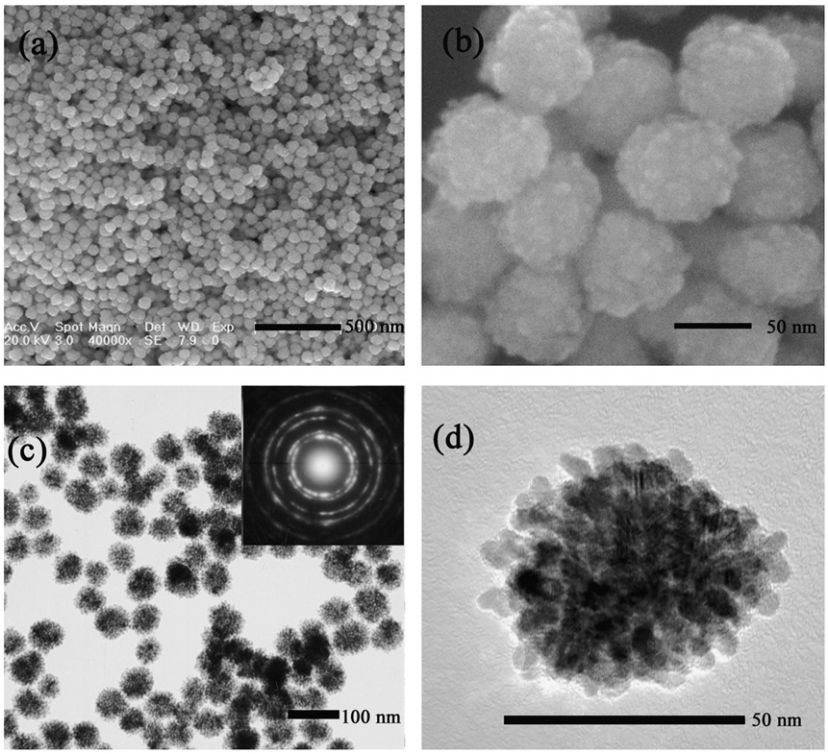

Fig. 1. Low and high-magnification SEM (a, b) and TEM (c, d) images of Pt nanospheres. The inset shows the selected-area electron diffraction patterns.

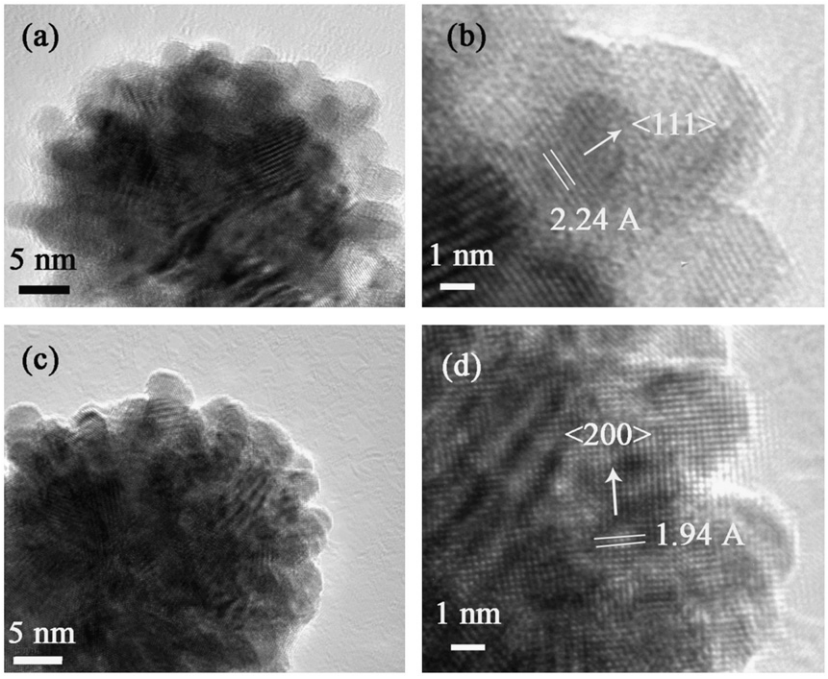

Fig. 2. High-magnification TEM images (a, c) and HRTEM images (b, d) of Pt nanospheres.

consistent with the reported value in JCPDS card (0.392 nm; no. 04-0802).

XPS was carried out to investigate the surface compositions of large Pt nanospheres. XPS spectrum were shown in Fig.4. XPS analysis of these nanospheres indicated significant Pt 4*f* signal corresponding to binding energy of metallic platinum [30–31]. Moreover, the binding energy located at 37.8 and 35.4 eV could be attributed to W $5p_{3/2}$ and W $4f_{7/2}$ of the $SiW_{12}O_{40}^{4-}$ anions, respectively, suggesting that the $SiW_{12}O_{40}^{4-}$ anions adsorbed onto the surface of Pt nanospheres and existed in the oxidized form [15]. It could be argued that the XPS spectrum of W was derived from the existence of silicotungstate or the $SiW_{12}O_{40}^{4-}$ anions still remained its structure after reaction. The FTIR analysis (Fig. S1) showed that the absorbance of the reaction production after

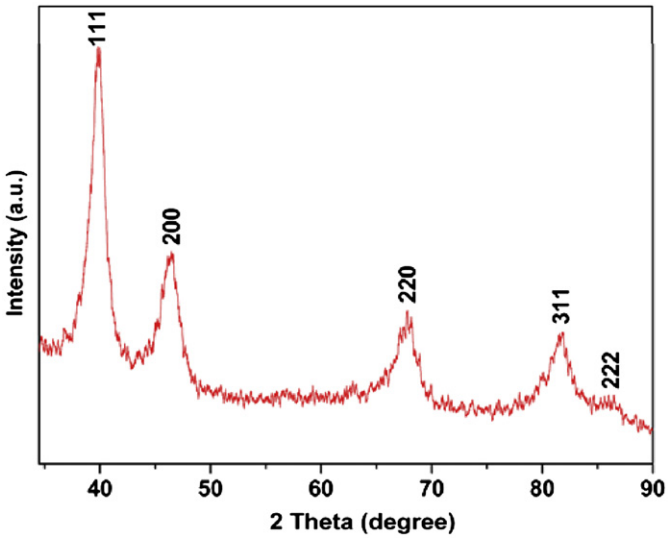

Fig. 3. X-ray diffraction patterns of the platinum nanospheres.

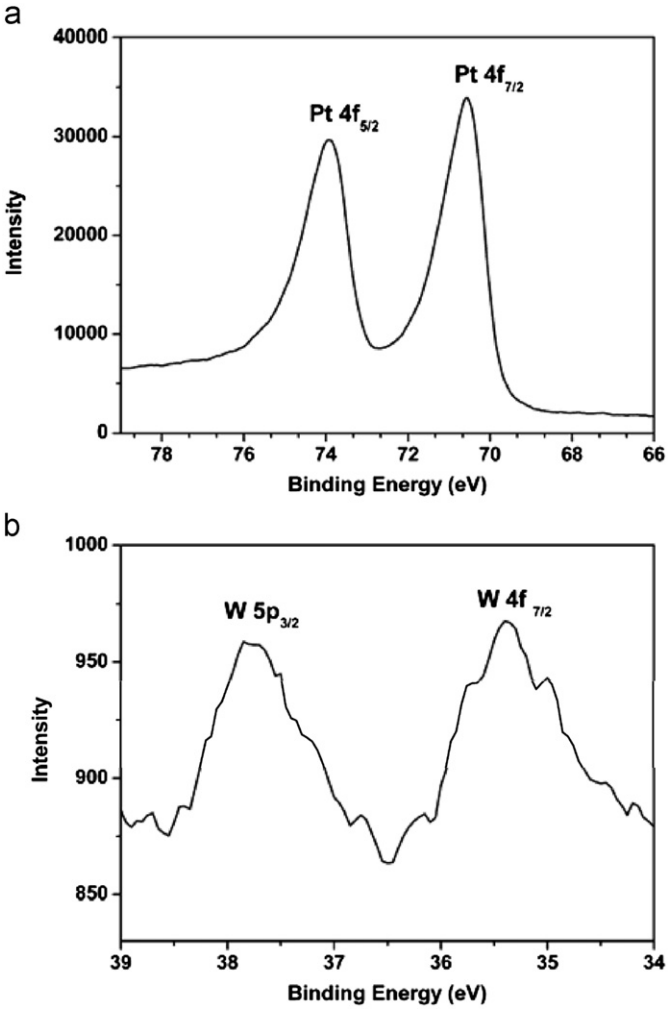

Fig. 4. XPS spectra of Pt nanospheres: (a) Pt 4*f* level and (b) W 5*p* and W 4*f* level.

forming Pt nanospheres was almost consistent with $H_4SiW_{12}O_{40}$ [32], revealing that $SiW_{12}O_{40}^{4-}$ anions remained their structure after the reaction.

3.2. Effect of experimental parameters on the reaction rate and Pt nanospheres

Several experimental parameters had been investigated to explore their role in the fabrication of Pt nanospheres. It was found that the reaction rate could be controlled by adjusting the concentration of HSiW. When fixed the concentration of H_2PtCl_6 and AA, the HSiW/H_2PtCl_6 molar ratio was varied from 0 to 10. In the absence of HSiW, the reduction of H_2PtCl_6 at room temperature was much slower. However, upon addition of HSiW, the reduction process under the same conditions became faster obviously, and showed an increasing trend with the increase of HSiW/H_2PtCl_6 molar ratio (Table S1). According to these results and earlier studies [33], we postulated that HSiW could catalyze the reduction of $PtCl_6^{2-}$ by AA due to HSiW-mediated electron transfer from AA to $PtCl_6^{2-}$. It might be attributed to the unique electronic characteristics and structural robustness of POMs in that they could gain and donate electrons while keeping their structure unchanged. In general, an increasing HSiW/H_2PtCl_6 molar ratio leaded to the formation of smaller nanodots (Fig. S2), but the size of large Pt nanospheres exhibited a contrary trend (Fig. 5). It is widely accepted that for the growth of nanocrystals their final size is determined by the nucleation rate and the growth rate at the initial stage of the chemical reaction [34]. In our case, an increase in the HSiW concentration (higher HSiW/H_2PtCl_6 molar ratio) increased the reduction rate, whereas the growth rate decreased at the same time due to the stabilizing agent role of HSiW. As a result, the formation of smaller nanodots could be expected. As for the contrary trend of large Pt nanospheres, it might be due to more POM polyanions doped in the Pt nanostructures when the HSiW concentration (higher HSiW/H_2PtCl_6 molar ratio) increased.

In our control experiments, the Pt nanostructures with similar morphology were formed (Fig. S2). However, these nanostructures were apt to aggregate and subsequently precipitated from the suspension due to typical hydrophobic surface property. It was worth noting that the formed colloid was stable without precipitating for several weeks in the presence of HSiW. Even if the precipitation happened, the Pt nanospheres can be easily redispersed by simply hand shaking. These observations indicated that HSiW play a role of stabilizer in the formation of such platinum nanostructures. It might be due to the POM polyanions adsorbing onto the surface of Pt nanodots, which provided both kinetic stabilization through coulombic repulsion between negatively charged particles and steric stabilization. In the previous study on iridium colloid, the highly charged POM macroanions exhibited a better ability to stabilize metal nanoparticles than other types of anions [35]. Moreover, it was found that the concentration of AA had a significant effect on the compact pattern of small nanodots. In other word, the packing density of large Pt nanospheres could be tuned by controlling the concentration of AA. As shown in Fig. S4, when the reaction was conducted with lower concentration of AA, the closely packed nanospheres could be produced. In contrast, increasing the amount of AA yielded the formation of loosely packed nanospheres. The possible reason was that more AA molecules could be adsorbed onto the surface of small Pt nanodots due to its higher concentration in the media, leading to bigger interdot space. Although the solid-state TEM was the ex-situ examination, the images could reflect the relative packed situation in the solution. These results further supported the fact that AA acted as a structure-directing agent by virtue of its flexible molecular conformations.

The concentration of platinum precursor had also been investigated to explore its effect on the morphological feature of Pt nanospheres. Fig. S5 showed typical TEM images of the Pt

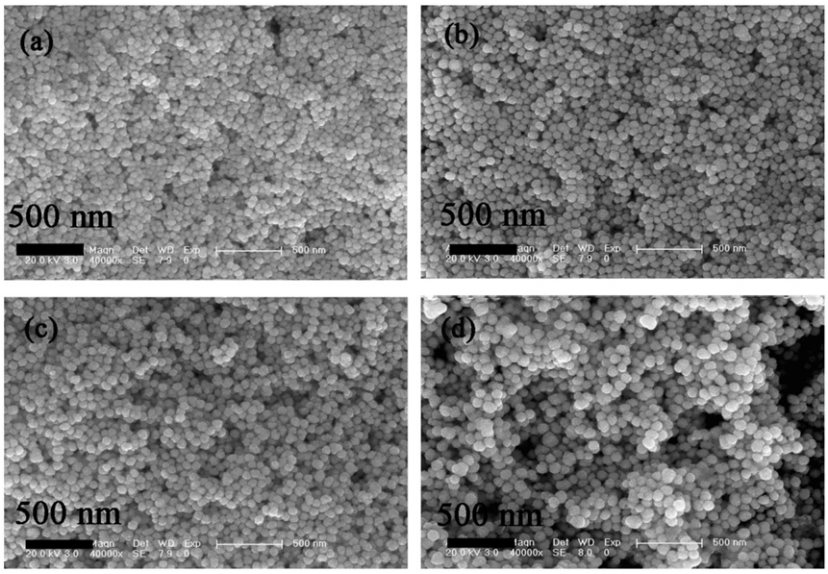

Fig. 5. SEM images of Pt nanospheres obtained upon reduction of 0.32 mmol L^{-1} H_2PtCl_6 by 33 mmol L^{-1} AA at different HSiW/H_2PtCl_6 molar ratio: (a) 0.1, (b) 1.0, (c) 5.0 and (d) 10.0.

nanospheres prepared at different HSiW/H_2PtCl_6 molar ratio of 50:1, 2:1, and 1:2 when fixed AA and HSiW concentration. Interestingly, the average diameter of Pt nanospheres did not obviously change and the morphology was also kept uniform. All the above reactions under different conditions supported the fact that the Pt nanodots tended to aggregate into nanospheres with almost uniform diameters.

In addition, the effect of reaction temperature on the formation of pt nanospheres were investigated in the presence and absence of HSiW at different temperatures and the resultant products are analyzed by SEM (Fig. S6. Upon increasing the temperature to 80 °C, the Pt nanospheres were formed in several minutes in both systems. However, the Pt nanostructure formed in the system of absence of HSiW almost completely precipitated from the suspension after several minutes. The experimental results indicate that a higher temperature is in favor of the reduction of H_2PtCl_6 with AA, and although the HSiW did not obviously exhibite the catalytic activity towards the reduction of H_2PtCl_6 with AA, it still played an important role in stablizing the Pt nanospheres.

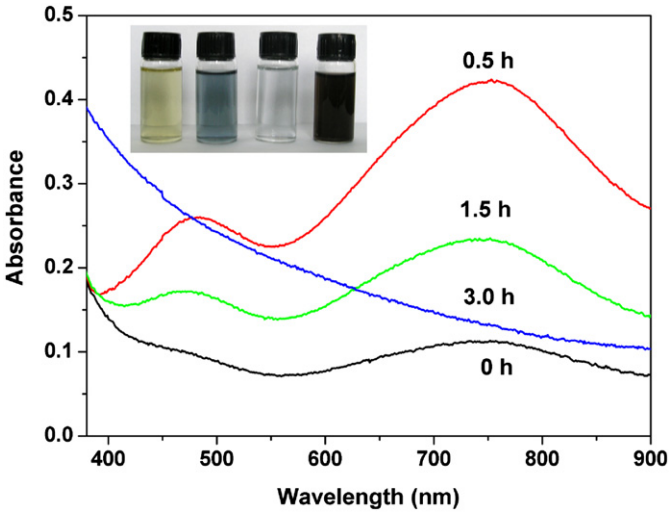

Fig. 6. The UV–vis absorption spectra of the reduction of H_2PtCl_6 (4.8×10^{-4} M) by AA (50 mM) using HSiW (5 mM) as assisting agent recorded at different reaction state. The inset shows the corresponding optical images.

3.3. Formation mechanism

In order to understand the formation mechanism of Pt nanospheres, we conducted UV–vis spectrum over time. The intense absorption of the reduced POMs and the weak surface plasmon absorption of the Pt nanoparticles in the same spectral region (Fig. 6) offered the idea conditions to follow the course of the reduction reaction simply by UV–vis absorption. The absorption bands characteristic of the reduced POMs (heteropoly blue) at 480 and 750 nm appear within 2 min upon addition of POMs, suggesting that POMs was preferentially reduced by AA [36]. The blue color of the solution gradually disappeared as the reaction proceed, followed by a sudden change to dark brown. These phenomena indicate that the reduction of the Pt^{4+} species at the initial stage was very slow, and further reduction was obviously accelerated as soon as the nucleation of Pt^0 particles started. Based on the above results, the overall reduction was believed to proceed in two steps, involving that an one-electron reduction of HSiW with AA (Eq. (1)), followed by re-oxidation of the reduced POMs with the metal cations to yield the metal nanospheres (Eq. (2)). The net balanced reaction was Eq. (3) obtained by adding Eq. (1) and Eq. (2), indicating that HSiW acted as the redox/electron transfer catalyst for shuttling the ascorbic acid reducing agent electrons to the Pt^{4+} in-situ. The oxidation of AA was confirmed by MS analysis. As shown in Fig. S7, the peak at 172.9 and 174.0 was attributed to the dehydroascorbic acid, suggestting that AA acted as the reductant during the formation of Pt nanospheres.

Considering the redox potentials of $PtCl_6^{2-}/Pt^0$ (0.725 V vs. NHE) and $SiW_{12}O_{40}^{4-}/SiW_{12}O_{40}^{5-}$ (0.057 V vs. NHE) couples, $PtCl_6^{2-}$ should be preferentially reduced by AA [37]. In the present case, however, they did not follow the above-mentioned sequence. As we all know, the redox potential just responds a thermodynamic trend, which did not involve any kinetics. If we assumed a kinetic control, it should be reasonable that the reduction of HSiW happened in advance because an one-electron transfer for Eq. (1) was kinetically much easier than a four-electron transfer for Eq. (2) [38].

On the basis of the above results and the autocatalytic mechanism of Finke [10], a four-step formation mechanism was proposed to explain how the large Pt nanospheres were produced, as schematically shown in Scheme 1. Step I: Slow continous formation of Pt nuclei. POMs accelerated the reduction of H_2PtCl_6 with AA under acidic conditions by mediating electron transfer from AA to $PtCl_6^{2-}$, leading to produce Pt^0 species. Step II: Fast autocatalytic surface growth. As found for Pt^{4+} species in solution, the appearance of long induction time indicated that the further reduction of Pt was autocatalytic [31]. When the Pt nuclei reached a certain size (~500 atoms), they apparently became autocatalytic for the further reduction of platinum [39]. Therefore, these Pt nuclei rapidly grew into nanodots as the autocatalytic reduction exhausted the available platinum precursor. A similar mechanism based on slow, continuous nucleation and fast autocatalytic growth had previously been proposed to explain the formation of platinum nanodendrites [5]. Step III: The aggregation of primary Pt nanodots. Generally, nanostructure formation after fast nucleation in solution typically relates to two mechanisms: Ostwald ripening and aggregation [40]. Ostwald ripening refers to the processes where larger particles grow at the expense of smaller ones, and it is generally believed to experience a longer time for further crystal growth. In this case, however, once the nucleation of Pt^0 particles occurred, the further formation of the Pt nanospheres was very quick so that we could not capture the intermediate stage. Furthermore, the Pt nanospheres obviously consisted of small primary nanodots according to TEM images.

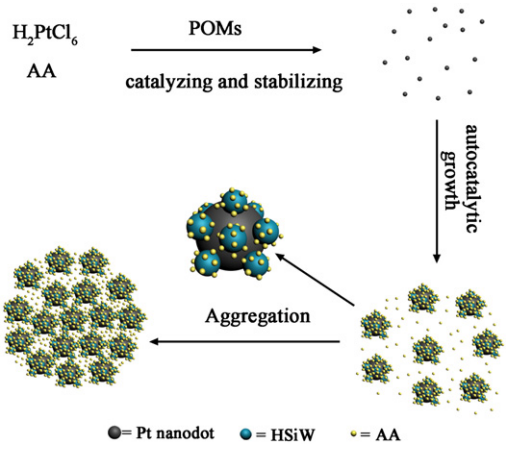

Scheme 1. Schematic mechanism for forming the large Pt nanospheres.

Based on these observations, it was reasonable to speculate that Pt nanospheres were formed mainly by an aggregation route using AA molecules as a structure-directing agent, rather than Ostwald ripening mechanism. This speculation was supported by the fact that the compact form of Pt nanospheres could be affected by AA concentration. Step VI: Autocatalytic agglomeration between small Pt nanodots and large Pt nanospheres. This step was deduced according to the most general mechanism to date by which transition-metal nanoparticles nucleate, grow and agglomerate to bulk metal under conductive conditions.

Recently, Nadjo et al. found that two polyoxomolybdate cyclic compounds were very efficient both as reductants of Pt and Pd metallic salts and as capping agents for the resulting Pt^0 and Pd^0 nanoparticles [41]. In their case, a limited number of urchin-like structure were observed. They proposed a gradual coalescence mechanism by which small-size nanoparticles aggregate to build up large crystallites. Compared with the previous work, the advantage of the proposed method is the in-situ use of the POM as the redox/electron transfer catalyst for shuttling the ascorbic acid reducing agent electrons to the Pt^{4+}.

3.4. Electrocatalysis of Pt nanospheres toward methanol oxidation

Considering the assembling structure of Pt nanosphere with rough surface, it will be very interesting to explore their application as electrocatalysts. In this case, the oxidation of methanol was utilized to examine the electrocatalytic behaviors of Pt nanospheres. As observed in Fig. S8, the well-defined hydrogen adsorption/desorption (−0.20 to 0.10 V) and platinum oxides reduction peaks show up, characteristic of Pt-based electrodes, indicating that Pt nanospheres were fixed on the surface of GC electrode. The activities of Pt nanospheres toward methanol oxidation were estimated in 0.5 M H_2SO_4 and 1.0 M CH_3OH aqueous solution. Fig. 7(A) showed the cyclic voltammograms of CH_3OH oxidation on Pt nanospheres (a) and commercial Pt/C catalyst (40 wt% Pt) (b) modified GC electrode with the same Pt loadings at a scan rate of 100 mV S^{-1}. The current peak in the forward scan was attributed to CH_3OH electrooxidation at the modified electrode. In the reverse scan, the oxidation peak was probably associated with the removal of the residual carbon species formed in the forward scan. For Pt nanospheres catalyst, the CH_3OH oxidation current peak appeared at about 0.68 V in the anodic scan, which was lower than that of the commercial Pt/C catalyst (0.71 V). Also, it was found that the current density of Pt nanosphere was approximately 2.36 times higher than that of Pt/C catalyst. This lower anodic overpotential and higher current

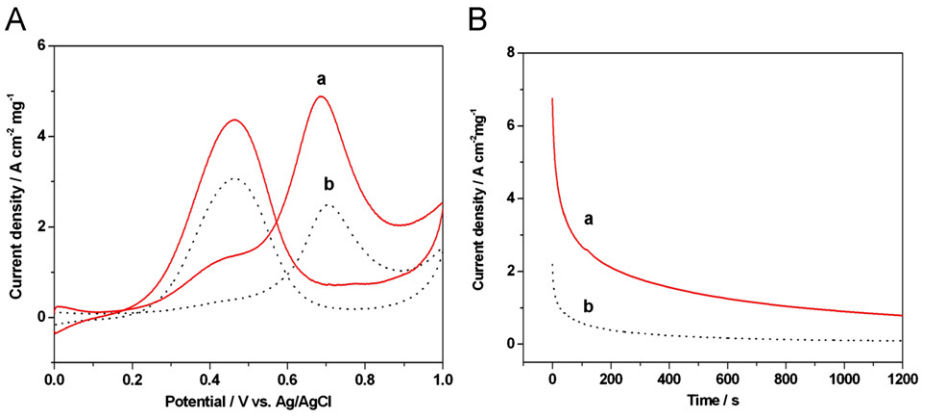

Fig. 7. (A) Cyclic voltammograms of CH_3OH oxidation at Pt nanospheres (a) and Pt/C catalyst (b) modified GC electrode in a 0.5 M H_2SO_4 solution containing 1 M CH_3OH with a scan rate of 100 mV/s. (B) Current density–time curves of Pt nanospheres (a) and Pt/C catalyst (b) modified GC electrode in a 0.5 M H_2SO_4 solution containing 1 M CH_3OH at 0.7 V.

density for the Pt nanospheres revealed that the as-synthesied Pt nanospheres exhibited higher electrocatalytic activity than that of commercial Pt/C catalyst. Actually, the HSiW can also perform the similar electrocatalytic function as that of Pt [42], so the electrocatalytic activity of HSiW was investigated. Fig. S9 showed the cyclic voltammograms of CH_3OH oxidation on Pt nanospheres (a) and HSiW with the same amount in Pt nanospheres (b) modified GC electrode at a scan rate of 100 mV S^{-1}. The HSiW did not exibite obvious electrocatalytic activity toward the CH_3OH oxidation at the lower concentration, suggesting that the higher electroncatalytic activity of Pt nanospheres did not benefited from HSiW but from Pt.

From the viewpoint of practical application, it was very important to investigate the tolerance of the catalyst to the poisoning species, Pt═C═O. According to earlier work, the ratio of the forward oxidation current peak (I_f) to the reverse current peak (I_b), I_f/I_b, was considered to be an index of the catalyst tolerance to the poisoning species. In this case, the I_f/I_b ratio of Pt nanospheres was calculated to be 1.13, which was 1.4 times higher than that of the commercial Pt/C catalyst (0.80), and thus suggesting that these Pt modified electrodes possessed better CO tolerance due to the less accumulation of incompletely oxidized carbonaceous species on the surface of Pt nanostructure. Fig. 7B indicated the chronoamperometric curves obtained from the above-mentioned electrodes at 700 mV. The current density for Pt nanospheres (line a) at 1000 s was 7.5 times than that of commercial Pt/C catalyst (line b). The above electrocatalytic data revealed that the as-prepared Pt nanospheres possessed better electrocatalytic activity and CO tolerance ability towards CH_3OH oxidation relative to the commercial Pt/C catalyst, which might be ascribed to their higher surface-to-volume ratios and enough absorption sites and better dispersibility [43].

4. Conclusions

We demonstrated that Pt nanospheres with controlled size and compact pattern could be synthesized by a new POMs-assisted approach. Importantly, it was found that POMs play a crucial role in controlling the reaction rate and stabilizing Pt nanospheres, which may be of importance in understanding the physical processes involved and provide new possibilities for design of novel metal nanostructures. Due to their unique nanostructures, these Pt nanosheres exhibited good electrocatalytic activity toward the oxidation of methanol and could be used as a promising nanoelectrocatalyst.

Acknowledgments

This work was supported by the National Science Foundation of China (no. 20371011/21003013), the Science and Technology Development Project Foundation of Jilin Province (no. 20060420), the Testing Foundation of Northeast Normal University (no. 201586000/201372000), the Ph.D. Station Foundation of Ministry of Education (no. 20060200002) and Science Foundation for Young Teachers of Northeast Normal University (no. 20070302/20070312).

Appendix A. Supplementary material

Supplementary data associated with this article can be found in the online version at doi:10.1016/j.jssc.2010.08.039.

References

[1] B. Lim, M.J. Jiang, P.H.C. Camargo, E.C. Cho, J. Tao, X.M. Lu, Y.M. Zhu, Y.N. Xia, Science 324 (2009) 1302–1305.
[2] L. Wang, Y. Yamauchi, J. Am. Chem. Soc. 131 (2009) 9152–9153.
[3] N.C. Bigall, T. Hartling, M. Klose, P. Simon, L.M. Eng, A. Eychmuller, Nano Lett. 8 (2008) 4588–4592.
[4] Y.J. Song, R.M. Garcia, R.M. Dorin, H.R. Wang, Y. Qiu, E.N. Coker, W.A. Steen, J.E. Miller, J.A. Shelnutt, Nano Lett. 7 (2007) 3650–3655.
[5] Y.J. Song, Y. Yang, C.J. Medforth, E. Pereira, A.K. Singh, H.F. Xu, Y.B. Jiang, C.J. Brinker, F.V. Swol, J.A. Shelnutt, J. Am. Chem. Soc. 126 (2004) 635–645.
[6] H.P. Liang, H.M. Zhang, J.S. Hu, Y.G. Guo, L.J. Wan, C.L. Bai, Angew. Chem. Int. Ed. 43 (2004) 1540–1543.
[7] Y. Yamauchi, A. Takai, T. Nagaura, S. Inoue, K. Kuroda, J. Am. Chem. Soc. 130 (2008) 5426–5427.
[8] B. Lim, M.J. Jiang, J. Tao, P.H.C. Camargo, Y.M. Zhu, Y.N. Xia, Adv. Funct. Mater. 18 (2008) 1–12.
[9] (a) Y. Lin, R.G. Finke, J. Am. Chem. Soc. 116 (1994) 8335–8353;
(b) Y. Lin, R.G. Finke, Inorg. Chem. 33 (1994) 4891–4910;
(c) J.D. Aiken III, Y. Lin, R.G. Finke, J. Mol. Catal. A: Chem. 114 (1996) 29–51.
[10] (a) C. Besson, E.E. Finney, R.G. Finke, Chem. Mater. 17 (2005) 4925–4938;
(b) C. Besson, E.E. Finney, R.G. Finke, J. Am. Chem. Soc. 127 (2005) 8179–8184;
(c) E.E. Finney, R.G. Finke, Chem. Mater. 20 (2008) 1956–1970.
[11] A. Troupis, A. Hiskia, E. Papaconstantinou, Angew. Chem. Int. Ed. 41 (2001) 1911–1914.
[12] S. Mandal, P.R. Selvakannan, R. Parischa, M. Sastry, J. Am. Chem. Soc. 125 (2003) 8440–8441.
[13] B. Keita, T.B. Liu, L. Nadjo, J. Mater. Chem. 19 (2009) 19–33.
[14] Z.H. Kang, Y. Liu, C.H.A. Tsang, D.D.D. Ma, E.B. Wang, S.T. Lee, Chem. Commun. (2009) 413–415.
[15] J. Zhang, B. Keita, L. Nadjo, I.M. Mbomekalle, T.B. Liu, Langmuir 24 (2008) 5277–5283.
[16] Z.H. Kang, C.H.A. Tsang, Z.D. Zhang, M.L. Zhang, N.B. Wong, J.A. Zapien, Y.Y. Shan, S.T. Lee, J. Am. Chem. Soc. 129 (2007) 5326–5327.
[17] Z.H. Kang, E.B. Wang, B.D. Mao, Z.M. Su, L. Gao, S.Y. Lian, L. Xu, J. Am. Chem. Soc. 127 (2005) 6534–6535.
[18] B.D. Mao, Z.H. Kang, E.B. Wang, C.G. Tian, Z.M. Zhang, C.L. Wang, Y.L. Song, M.Y. Li, J. Solid State Chem. 180 (2007) 497–503.
[19] B.D. Mao, Z.H. Kang, E.B. Wang, C.G. Tian, Z.M. Zhang, C.L. Wang, S.H. Li, Chem. Lett. 36 (2007) 70–71.
[20] Q.Y. Li, Z.H. Kang, B.D. Mao, E.B. Wang, C.L. Wang, C.G. Tian, S.H. Li, Mater. Lett. 62 (2008) 2531–2534.
[21] Q.Y. Li, E.B. Wang, S.H. Li, C.L. Wang, C.G. Tian, G.Y. Sun, J.M. Gu, R. Xu, J. Solid State Chem. 182 (2009) 1149–1155.
[22] A. Sanyal, M. Sastry, Chem. Commun. (2003) 1236–1237.
[23] S. Mandal, D. Rautaray, M. Sastry, J. Mater. Chem. 13 (2003) 3002–3005.
[24] S. Mandal, A. Das, R. Srivastava, M. Sastry, Langmuir 21 (2005) 2408–2413.
[25] B. Keita, I.M.M. Mbomekalle, L. Nadjo, C. Haut, Electrochem. Commun. 6 (2004) 978–983.
[26] B. Keita, G. Zhang, A. Dolbecq, P. Mialane, F. Secheresse, F. Miserque, L. Nadjo, J. Phys. Chem. C 111 (2007) 8145–8148.
[27] G. Zhang, B. Keita, A. Dolbecq, P. Mialane, F. Secheresse, F. Miserque, L. Nadjo, Chem. Mater. 19 (2007) 5821–5823.
[28] M.T. Pope, A. Müller, Polyoxometalate Chemistry, Netherlands, 2001.
[29] H.P. Klug, L.E. Alexander, in: X-ray Diffraction Procedures for Polycrystalline and Amorphous Materials, Wiley, New York, 1974.
[30] L.X. Zhang, L. Wang, S.J. Guo, J.F. Zhai, S.J. Dong, E.K. Wang, Electrochem. Commun. 11 (2009) 258–261.
[31] J.Y. Chen, T. Herricks, M. Geissler, Y.N. Xia, J. Am. Chem. Soc. 126 (2004) 10854–10855.
[32] A. Teze, G. Herve, in: A.P. Ginsberg (Ed.), Inorganic Synthesis, vol. 27, John Wiley & Sons, New York1990, p. 91.
[33] L.H. Lu, H.S. Wang, S.Q. Xi, H.J. Zhang, J. Mater. Chem. 12 (2002) 156–158.
[34] (a) M.A. Watzky, R.G. Finke, Chem. Mater. 9 (1997) 3083–3095;
(b) M.A. Watzky, E.E. Finney, R.G. Finke, J. Am. Chem. Soc. 130 (2008) 11959–11969.
[35] S. Ozkar, R.G. Finke, J. Am. Chem. Soc. 124 (2002) 5796–5810.
[36] T. Yamase, Chem. Rev. 98 (1998) 307–326.
[37] A. Troupis, E. Gkika, A. Hiskia, E. Papaconstantinou, C. R. Chim. 9 (2006) 851–857.
[38] L.M. Liz-Marzan, A.P. Philipse, J. Phys. Chem. 99 (1995) 15120–15128.
[39] E. Greenbaum, J. Phys. Chem. 92 (1988) 4571–4574.
[40] R.L. Penn, G. Oskam, T.J. Strathmann, P.C. Searson, A.T. Stone, D.R. Veblen, J. Phys. Chem. B 105 (2001) 2177–2182.
[41] A. Dolbecq, J.D. Compain, P. Mialane, J. Marrot, F. Secheresse, B. Keita, L.R.B. Holzle, F. Miserque, L. Nadjo, Chem. Eur. J. 15 (2009) 733–741.
[42] J.1. Wei, H. Yang, Y.G. Yang, Z.L. Zhang, Rare Met. Mater. Eng. 34 (2005) 959–961.
[43] L. Wang, S.J. Guo, J.F. Zhai, S.J. Dong, J. Phys. Chem. C 112 (2008) 13372–13377.